CHAPTER 2

Tau-p TRANSFORMATION

Seismic data are usually recorded and processed as a function of the traveltime (t) and source–receiver offset (x), so called time-space domain (t-x domain). The same data can also be represented by a plot of the slope (p) of events in t-x domain against the intercept on the time axis (τ), so called linear *tau-p* domain (Diebold and Stoffa, 1981). Whereas the Fourier transform represents data as a superposition of harmonics waves, the linear *tau-p* transformation represents the same data as a superposition of straight-line events. The straight-line events in t-x domain, such as the direct wave, headwave events, ground roll and air wave, transform to points and the hyperbolic reflections in t-x domain become ellipses in the linear *tau-p* domain (Telford *et al.*, 1990). Also, the seismic data can be represented by a plot of the curvature (q) of hyperbolic events in t-x domain against the intercept on the time axis (τ), so called parabolic *tau-p* domain. The parabolic *tau-p* transformation represents data as a summation over hyperbolic curved trajectory. Thus the hyperbolic events in t-x domain are transformed to points in parabolic *tau-p* domain

This chapter explains the mathematical relations of the seismic wave in t-x domain, linear *tau-p* domain and parabolic *tau-p* domain, follow by the application of the *tau–p* transform.

2.1 The seismic events in time-space domain

Consider a homogeneous layer model in Figure 2.1 (a) which has a single layer thickness h and velocity v_1 over a half-space velocity v_2. There are 3 simple seismic wave forms. The first is a direct wave (D), travels directly from a source to a sequence of receivers. The second is a refracted wave or headwave (H) (in the case of $v_1 < v_2$ only), travels from source and incidences at the critical angle (θ_c) at the higher

layer interface then travels along the interface with the velocity of the lower medium and refracted back to the surface. The third is a reflected wave (R), travels from source and incidences at the layer interface then reflected back to the surface. These waves are detected by the sequence of receiver with different distance from source and plotted in *t-x* domain, called shot record (Figure 2.1 (b)).

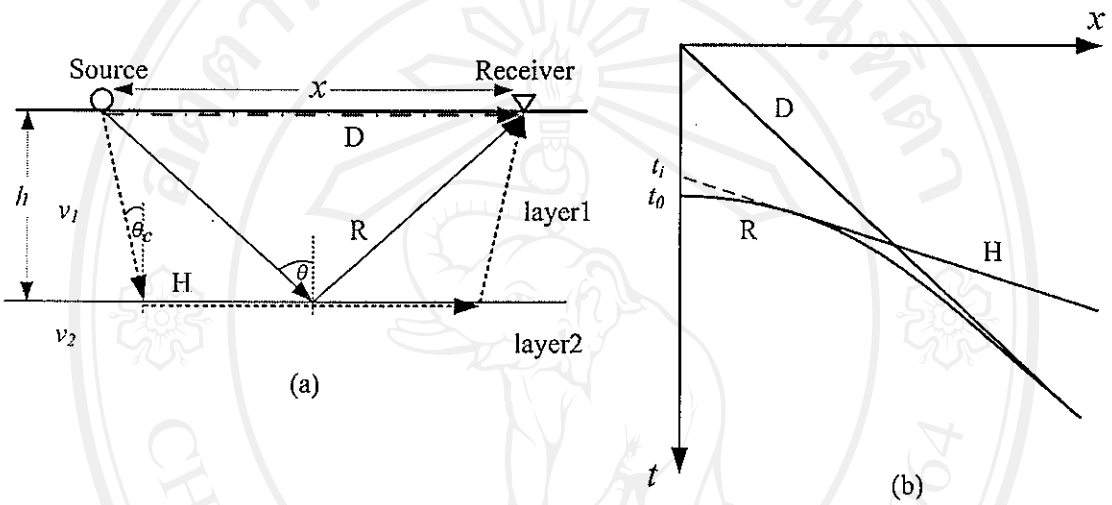

Figure 2.1 (a) The source-receiver geometry for a single layer model with $v_1 < v_2$. The ray path in the model can be detected by the series of receivers. (b) The shot record plotted in the *t-x* domain where D, H and R are the direct wave, the headwave and the reflected wave, respectively.

The linear travel time events, directed wave and headwave, can be expressed in the function of distance as

$$t = t_i + \frac{x}{f(v)} \quad , \tag{2.1}$$

where t_i is a intercept time and $f(v)$ is a velocity function.

In the case of the direct wave, $t_i = 0$ and the $f(v) = v_1$. Thus the direct wave traveltime (t_D) can be written as

$$t_D = \frac{x}{v_1} \quad . \tag{2.2}$$

For the headwave, $t_i = 2h\cos\theta_c / v_1$ and $f(v) = v_2$. Thus the headwave traveltime (t_H) can be written as

$$t_H = \frac{2h\cos\theta_c}{v_1} + \frac{x}{v_2} \quad . \tag{2.3}$$

The hyperbolic traveltime event, reflected wave, can be expressed in the function of distance as

$$t^2 = t_0^2 + \frac{x^2}{v_i^2} \quad , \tag{2.4}$$

where t_0 is the zero offset traveltime, source and receiver at the same position, or the normal incident traveltime, $t_0 = 2h/v_i$ and v_i is the velocity of the layer media, in this case $v_i = v_1$. Thus the reflected wave traveltime (t_R) can be written as

$$t_R^2 = \left(\frac{2h}{v_1}\right)^2 + \left(\frac{x}{v_1}\right)^2 \quad . \tag{2.5}$$

Rewriting the equation (2.4) by using a binomial expansion approximation of the square root, the hyperbolic traveltime event becomes the parabolic traveltime event (approximately to the second order of x) as

$$t = t_0\sqrt{1 + \frac{x^2}{t_0^2 v_i^2}} \quad , \tag{2.6}$$

$$t \approx t_0 + \frac{x^2}{2t_0 v_i^2} \quad . \tag{2.7}$$

Hence the hyperbolic event, equation (2.6), becomes approximately the parabolic event, equation (2.7). The traveltime formula for the multi-layer is shown in Appendix C.

2.2 The seismic events in *tau-p* domain

The *tau-p* transformation is a mathematical technique that has seen popular usage in seismic data processing and analysis. It is a processing tool utilized to exploit the differences in the moveout of seismic events. Variants of the algorithm are commonly employed in discriminating between primary reflections and other types of coherent noise.

The simplified formula for two-dimensional (2-D) generalized *tau-p* transformation is given as (Beylkin, 1987)

$$m(p,\tau) = \int\int d(x,t)\delta[t = t(\tau, p, x)]dtdx \quad , \tag{2.8}$$

where the function $d(x,t)$ is the input signal in time-space domain and $m(p,\tau)$ is the output function in *tau-p* domain. The Dirac delta function (δ) identifies rectilinear path that is a specified set of projection, given by t. The function t is particularly defined for the *tau-p* transformation.

2.2.1 The linear tau-p transformation

The linear *tau-p* transformation or slant-stack transformation involves summation along line (Thorson, 1978)

$$t = \tau + px \quad , \tag{2.9}$$

where τ is the intercept on the time axis and p is ray parameter, defined by

$$p = \frac{dt}{dx} = \frac{\sin\theta}{v_i} \quad , \tag{2.10}$$

where θ is dip angle of the ray path.

Hence the transformation in equation (2.8) can be written as

$$m(p,\tau) = \int\int d(x,t)\delta[t = \tau + px]dtdx \quad . \tag{2.11}$$

The inverse linear *tau-p* transformation may then be written as

$$d(x,t) = \int\int m(p,\tau)\delta[\tau = t - px]d\tau dp \quad . \tag{2.12}$$

The linear *tau-p* transformation is most easily treated in the temporal Fourier domain. Let $D(x,\omega)$ and $M(p,\omega)$ be the Fourier transformation of $d(x,t)$ and $m(p,\tau)$, respectively, where ω is angular frequency. The forward linear *tau-p* transform is given by

$$M(p,\omega) = \int D(x,\omega)e^{i\omega px}dx \ , \tag{2.13}$$

The inverse linear *tau-p* transformation is given by

$$D(x,\omega) = \int M(p,\omega)e^{-i\omega px}dp \ , \tag{2.14}$$

Case of the direct wave

Consider the direct wave traveltime, equation (2.2), can be written as

$$p = \frac{dt_D}{dx} = \frac{1}{v_1} \quad \text{and} \quad \tau = 0 \ .$$

Thus the direct wave, linear event in *t-x* domain, is transformed into a point ($\tau = 0, p = 1/v_1$) in the linear *tau-p* domain.

Case of the refracted wave

Consider the refracted wave traveltime, equation (2.3), where $v_1 < v_2$, can be written as

$$p = \frac{dt_H}{dx} = \frac{1}{v_2} \quad \text{and} \quad \tau = \frac{2h\cos\theta_c}{v_1} \ .$$

Thus the refracted wave, linear event in *t-x* domain, is transformed into a point ($\tau = \frac{2h\cos\theta_c}{v_1}, p = 1/v_2$) in the linear *tau-p* domain.

Case of the reflected wave

Consider the reflected wave traveltime, equation (2.5),

$$p = \frac{dt_R}{dx} = \frac{x}{v^2 t} \quad . \tag{2.15}$$

Replace $x = ptv^2$ to equation (2.5), which the results in

$$t = \frac{t_0}{\sqrt{1 - v^2 p^2}} \quad . \tag{2.16}$$

Replace $t = \frac{x}{pv^2}$ to equation (2.5), which the results in

$$x = \frac{v^2 p t_0}{\sqrt{1 - v^2 p^2}} \quad . \tag{2.17}$$

Solving the equation (2.9) by replaced t and x from equation (2.16) and (2.17), can be written as

$$\frac{\tau^2}{t_0^2} + v^2 p^2 = 1 \quad . \tag{2.18}$$

Equation 2.18 shows an ellipse equation when plot between p and τ with the major and minor axis length is $1/v$ and t_0, respectively. Thus the reflected wave, hyperbolic event in *t-x* domain, is transformed into ellipse in linear *tau-p* domain.

According to the linear *tau-p* transformation, the linear and hyperbolic events in *t-x* domain are transformed into some points and the elliptic events in the linear *tau-p* domain, respectively (Figure 2.2).

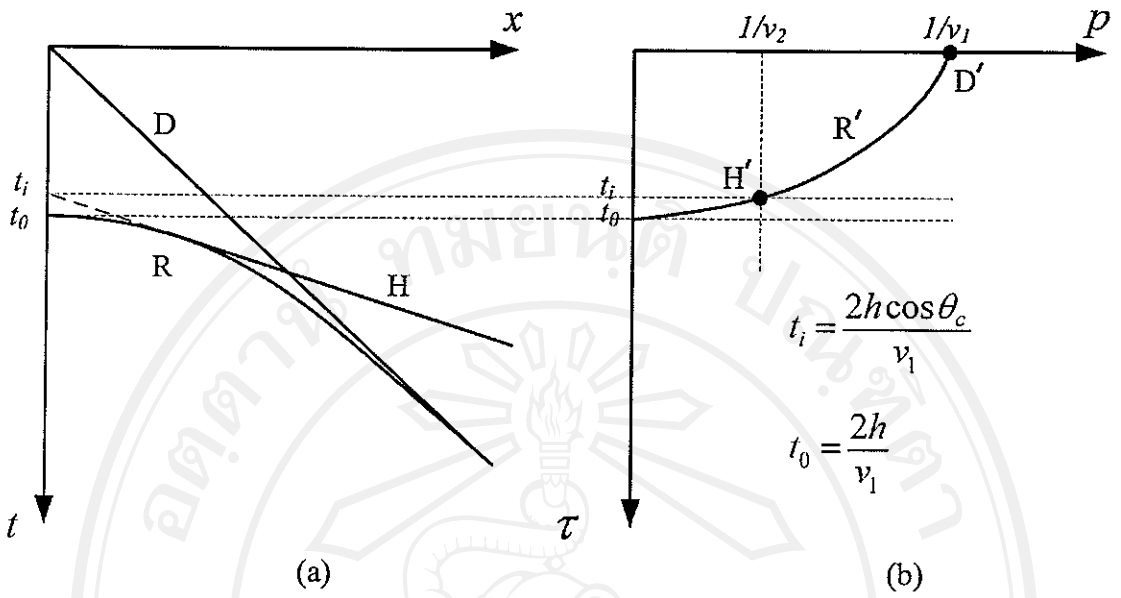

Figure 2.2 (a) Shot record in *t-x* domain. (b) Linear *tau-p* domain that transformed the direct wave D, the head wave H and reflected wave R transform into point D′, H′ and ellipse R′, respectively.

2.2.2 The parabolic tau-p transformation

The parabolic *tau-p* transformation involves summation along the parabolic curve (Hampson, 1986),

$$t = \tau + qx^2 \quad , \tag{2.19}$$

where q is the curvature variable representing the moveout of curve at offset. The transformation equation (2.8) can be written as

$$m(q,\tau) = \int\int d(x,t)\delta[t = \tau + qx^2]dtdx \quad . \tag{2.20}$$

The inverse parabolic *tau-p* transformation may then be written as

$$d(x,t) = \int\int m(q,\tau)\delta[\tau = t - qx^2]d\tau dq \quad . \tag{2.21}$$

Let $D(x,\omega)$ and $M(q,\omega)$ be the Fourier transformation of $d(x,t)$ and $m(q,\tau)$, respectively. The forward parabolic *tau-p* transformation is given by

$$M(q,\omega) = \int D(x,\omega) e^{i\omega q x^2} dx \quad . \tag{2.22}$$

The inverse parabolic *tau-p* transformation is given by

$$D(x,\omega) = \int M(q,\omega) e^{-i\omega q x^2} dq \quad . \tag{2.23}$$

From equation (2.20), the hyperbolic event in *t-x* domain, equation (2.7), is transformed into a point, $\tau = t_0$, $q = 1/2t_0 v_i$, in the parabolic *tau-p* domain. Consider five hyperbolic events P1, P2, P3, M1 and M2 in *t-x* domain (Figure 2.3 (a)) where P denote the primary events and M denote the multiples events, transformed to point P1′, P2′, P3′, M1′ and M2′ in parabolic *tau-p* domain (Figure 2.3 (b)). The moveout velocity of the event P1 < P2 < P3 and the moveout velocity of P1, M1 and M2 are the same.

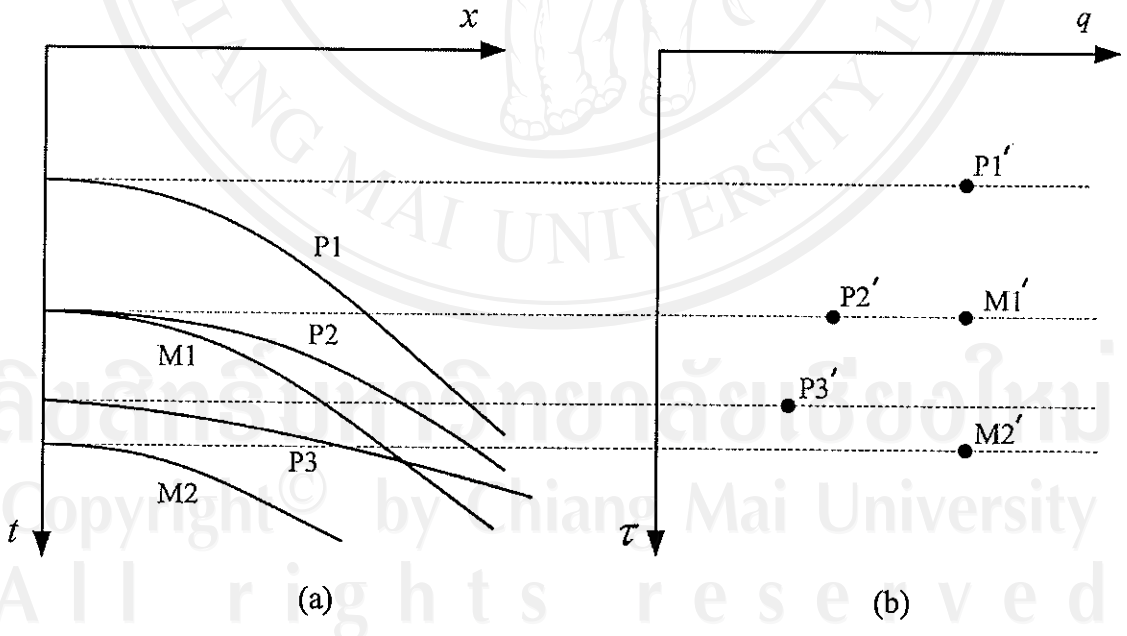

Figure 2.3 (a) Five hyperbolic events P1, P2, P3, M1 and M2 in *t-x* domain. (b) The parabolic *tau-p* domain showing the events in (a) transformed into points P1′, P2′, P3′, M1′ and M2′, respectively (modified from Yilmaz, 2001).

The *tau-p* transformation given in equation (2.8) is sufficient for use with continuous and infinite data. In practice, however, field data are finite and discretely sampled functions. Thorson and Claerbout (1985) used the idea of minimum entropy to formulate an expression to calculate the model space, m, for a finite number of q and τ. This formulation later was called the discrete Radon transform (DRT).

The computer-intensive time-domain DRT can be written as

$$m(p,\tau) = \sum_{i=1}^{N} \sum_{j=1}^{M} d(x_i, t_j) \quad , \tag{2.24}$$

where $i = 1,2,3,\ldots,\mathrm{N}$ and $j = 1,2,3,\ldots,\mathrm{M}$
The summation can be written in matrix from as

$$m = \boldsymbol{L}d \quad , \tag{2.25}$$

where $\boldsymbol{L}$ is matrix operator defined by the transformation curves of t', m is model space in matrix dimension $n_p \times n_\tau$ where n_p is number of velocity model, n_τ is number of time sample in t and d is input data in t-x domain in matrix dimension $n_x \times n_t$ where n_x is number of offset, n_t is number of time sampling. The element of the matrix operator, $\boldsymbol{L}$, dimensions are $n_x n_t \times n_v n_\tau$. The transformation in time-domain on field data is computer intensive and very costly due to calculations involving very large matrices. For an example field data set, $n_x = 60$, $n_t = 1000$, $n_p = 60$ and $n_\tau = 1000$; this implies a $\boldsymbol{L}$ matrix of dimension 60,000 × 60,000 (Yilmaz, 2001).

Sloving the problem of equation (2.25) requires a very large matrix by performing integration for independent frequencies in the Fourier domain. This methodology relies on the similarity of the integration over curved lines in the time domain to the integration over the stretch variable t in the Fourier domain. A forward Fourier transform is applied to the data and the transform equivalent to equation (2.13) and (2.22) for a given summation curve, $t = \tau + pf(x)$, is written as

$$M(p_j,\omega)=\sum_{k=1}^{N}D(x_k,\omega)e^{i\omega p_j f(x_k)} \quad , \tag{2.26}$$

where the function $f(x)$ is dependent upon the type of the transformation being computed and is usually given as x and x^2 for linear and parabolic *tau-p* transformation, respectively. The summation can be written in an equivalent matrix form as

$$M=\bar{L}^{A}D \quad , \tag{2.27}$$

where $\bar{L}^{A}$ is the adjoint of the Fourier-domain linear operator, $\bar{L}$. $\bar{L}$ is now defined as

$$\bar{L}_{k,j}=e^{-i\omega p_j f(x_k)} \quad . \tag{2.28}$$

Flow chart for the linear and parabolic *tau-p* forward transformations based on the above derivation is shown in Figure 2.4.

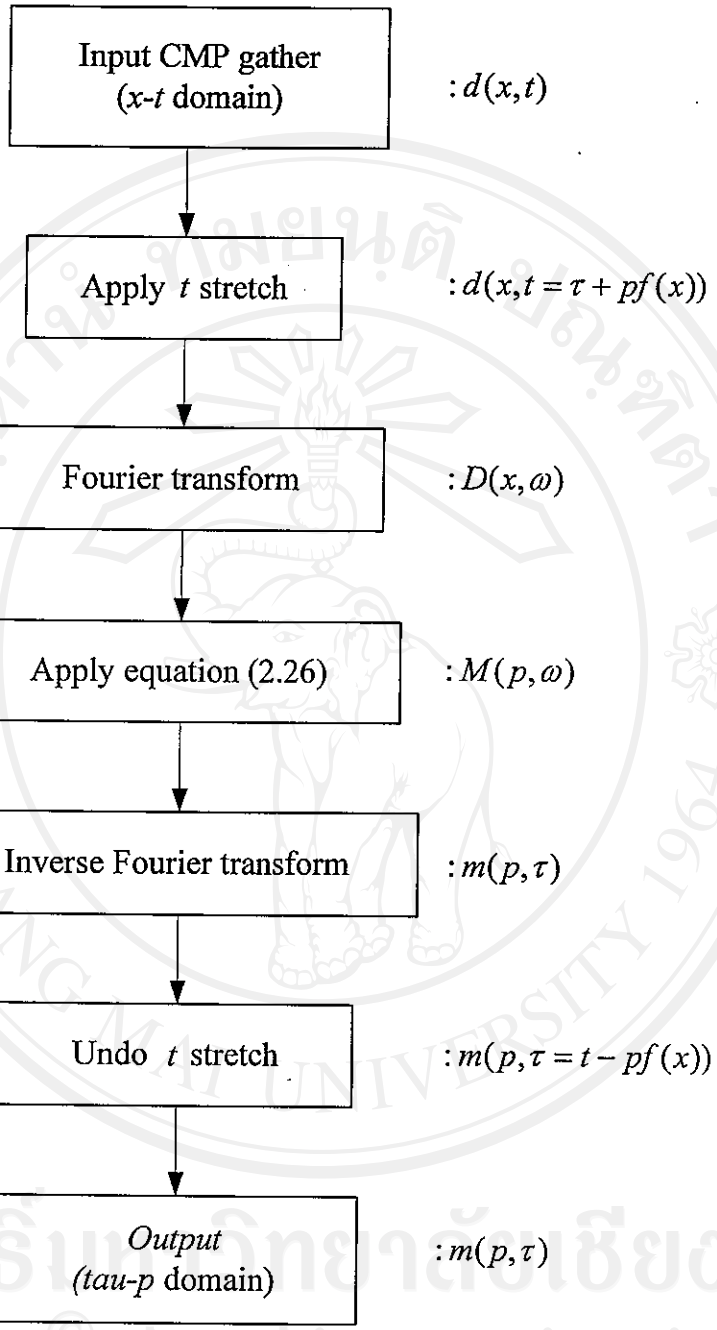

Figure 2.4 The flow chart of forward *tau-p* transformation. The function $f(x)$ is given by x and x^2 for linear and parabolic *tau-p* transformation, respectively (modified from Zhou and Greenhalgh, 1994).

2.3 Hyperbolic velocity filter

The limited aperture of the recording geometry and the spatial data sampling might considerably affect the separability of primaries and multiples (Kabir and Marfurt, 1999). This data sampling issue is called data aliasing. It causes many artifacts that dramatically affect focusing in the *tau-p* domain. A second source of problems can stem from aliasing of the *tau-p* transformation operator. The operator aliasing creates noise in the *tau-p* domain by the summation action (Abma *et al.*, 1999; Lumley *et al.*, 1994).

In 1981, Tatham *et al.* introduced the concept of hyperbolic velocity filtering (HVF) as a way to reduce aliasing in the linear *tau-p* transform. This technique is applied during the forward linear *tau-p* transformation of field records by muting the aliasing zone. The result after applied HVF, the signal-to-noise ratio (S/N) is improved and thus the full advantages of the linear *tau-p* domain can be utilized for further processing.

Following Tatham *et al.* (1981), differentiate equation (2.4) with respect to x and note that the ray parameter is given by $p = dt_R/dx$, thus will obtain

$$p = \frac{x}{tv^2} \quad . \tag{2.29}$$

By associating a velocity range (v_{min}, v_{max}) with each point (x, t), a limited range of p values can be determined from equation (2.29) by the inequalities

$$\frac{x}{tv_{max}^2} \le p \le \frac{x}{tv_{min}^2} \quad . \tag{2.30}$$

The velocity values v_{min} and v_{max} associated with the point (x, t) are chosen so that all geophysically possible stacking velocities associated with this point are within this chosen range. In practice, the velocities v_{min} and v_{max} are replaced by their time-variant equivalents $v_{min}(x, t)$ and $v_{max}(x, t)$, given by

$$v_{min}(x,t) = (1-k)v(x,t) \quad , \tag{2.31}$$

and $$v_{\max}(x,t) = (1+k)v(x,t) \quad , \tag{2.32}$$

where k is a specified fractional percentage value (usually between 15 percent and 25 percent)(Kelamis and Mitchell, 1990) of the primary velocity function, and $v(x, t)$ is an interpolated stacking velocity, via the traveltime equation for offset x. Inequalities (2.30) describe the basic algorithm for hyperbolic velocity filtering. Muting process in the linear *tau-p* domain, replace $t = \tau + px$ to equation (2.29), the results are given by

$$p^2v^2x + pv^2\tau - x = 0 \quad . \tag{2.33}$$

Solving this equation for the ray parameter gives

$$p = -\frac{\tau}{2x} \pm \sqrt{\frac{\tau^2}{4x^2} + \frac{1}{v^2}} \quad . \tag{2.34}$$

The limit of p value in linear *tau-p* domain can be shown as:

$$-\frac{\tau}{2x} + \sqrt{\frac{\tau^2}{4x^2} + \frac{1}{v_{\max}{}^2}} \le p \le -\frac{\tau}{2x} + \sqrt{\frac{\tau^2}{4x^2} + \frac{1}{v_{\min}{}^2}} \quad . \tag{2.35}$$

Equation (2.35) presents the limit of p for each τ in linear *tau-p* domain. This can be achieved using an equivalent set of mutes applied in the linear *tau-p* domain (Kelamis and Mitchell, 1990). This muting zone is illustrated in Figure 2.5.

2.4 Antialiasing condition for the parabolic *tau-p* transformation

Aliasing of the operator can be avoided if limit the dips of the parabolic *tau-p* transformation summation path. This dip filtering can be easily implemented in the Fourier domain, which results in a simple frequency limit condition.

Antialiasing the operator is equivalent to dip-filtering the operator. The anti-aliasing conditions can be written (Abma *et al.*, 1999) as

$$f_{\max} \le \frac{1}{2\Delta T} \quad , \tag{2.36}$$

where ΔT is the local slope of the operator between two adjacent traces. The computation of parabolic *tau-p* transformation in local slope as

$$\Delta T = \frac{\partial t(q,x)}{\partial x}\Delta x \quad , \tag{2.37}$$

from parabolic *tau-p* transformation condition $t(q,x) = \tau + qx^2$ and then

$$\Delta T = 2qx\Delta x \quad , \tag{2.38}$$

where Δx is the input trace spacing. The antialiasing condition becomes

$$f_{\max} \le \frac{1}{4qx\Delta x} \quad , \tag{2.39}$$

$$\omega_{\max} \le \frac{\pi}{2qx\Delta x} \quad . \tag{2.40}$$

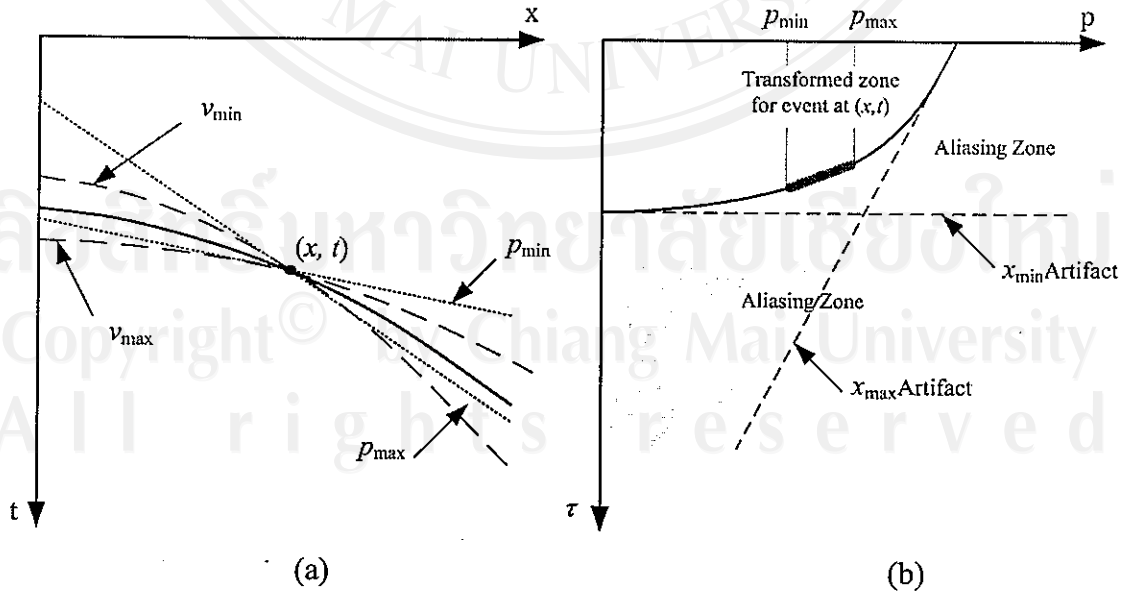

Figure 2.5 (a) A schematic of hyperbolic velocity filtering. (b) The muting zone in the linear *tau-p* domain (Dunne and Beresford, 1998).

2.5 Application of linear *tau-p* and parabolic *tau-p* transformation

The *tau-p* transformation is a processing tool utilized to exploit the differences in the moveout of seismic events. Variants of the algorithm are commonly employed in discriminating between primary reflections and other types of coherent noise. Linear *tau-p* processing is used in the suppression of linear noise events such as ground roll, direct wave, air wave and refraction wave (Trad *et al.*, 2002). The relationship between the linear *tau-p* transformation and the plane wave decomposition is also well established (Stoffa *et al.*, 1981; Treitel *et al.*, 1982). Least square procedures to compute the *tau-p* transformation were investigated by Thorson and Claerbout (1985), Beylkin (1987) and Kostov (1990). Parabolic *tau-p* processing is commonly employed in data interpolation and coherent noise attenuation such as multiples. The *tau-p* transform is advantageous because it requires no inherent knowledge of the coherent-noise-generating mechanism and works relatively well with non-uniform geometries (though it may require extensive computing time). Table 2.1 lists the main applications of the *tau-p* transformation in the seismic exploration.

Table 2.1 Application of the *tau-p* transformation in the seismic exploration (Zhou and Greenhalgh, 1994).

Application	References
Velocity analysis	Schultz and Claerbout, 1978; Schultz, 1982; Gray and Goldren, 1983
Migration and modeling	Chapman, 1978; Wenzel *et al.*, 1982; Miller *et al.*, Ruter, 1987
Inversion	Clayton and McMechan, 1981; Diebold and Stoffa, 1981; Thorson and Claerbout, 1985
Interpretation	McMechan and Ottolini, 1980; Kennett, 1981; Phinney *et al.*, 1981
Plane-wave decomposition	Stoffa *et al.*, 1981; Treitel *et al.*, 1982
Wave separation and/or filtering	Harland *et al.*, 1984; Moon *et al.*, 1986; Benoliel *et al.*, 1987; Hu and McMechan, 1987; Greenhalgh *et al.*, 1990
Noise attenuation	Alam and Austin 1981; Carraion, 1986; Noponen and Keeney, 1986; Hampson, 1986 & 1987; Yilmaz, 1989; Mitchell and Kelamins, 1990; Foster and Mosher, 1992; Zhou and Greenhalgh, 1993
Data interpolation	Lu, 1985
Controlled directional reception & controlled directional source methods	Zavalishin, 1982; Taner *et al.*, 1991; Sword, 1991

Hampson (1986) developed a demultiple technique for modeling parabolic events on NMO corrected CMP gathers that reduces the number of p-values necessary to model the reflections. This process flattens primary events with an NMO correction, leaving multiples approximately parabolic on the CMP gathers (Figure 2.6 (a)). A parabolic *tau-p* transform is applied to the data (Figure 2.6 (a)) and the multiples are muted in the parabolic *tau-p* domain. Hampson's technique is applied in this study for enhancing deep seismic signal and added rescaling (sign square) in parabolic *tau-p* domain for enhancing signal to random noise ratio.

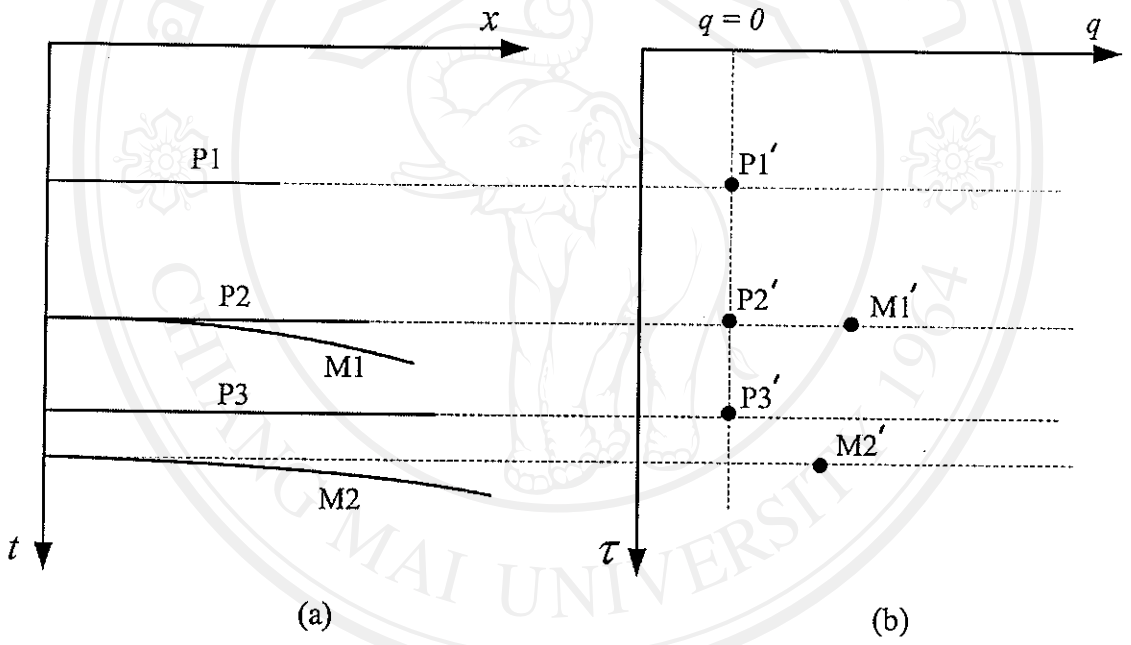

Figure 2.6 (a) The five reflectors in Figure 2.2 (a) after applying NMO correction by using reflection velocity function. (b) The parabolic *tau-p* domain after the reflectors in (a) P1, P2, P3, M1 and M2 are transformed into point P1′, P2′, P3′, M1′ and M2′ respectively.